AD-A124 247 CALCULATION OF TRANSONIC POTENTIAL FLOW AROUND A WING-BODY-TAIL COMBINATION(U) FLOW INDUSTRIES INC KENT WA J MERCER ET AL. APR 82 FR-227 N00014-80-C-0453 1/1

UNCLASSIFIED F/G 20/4 NL

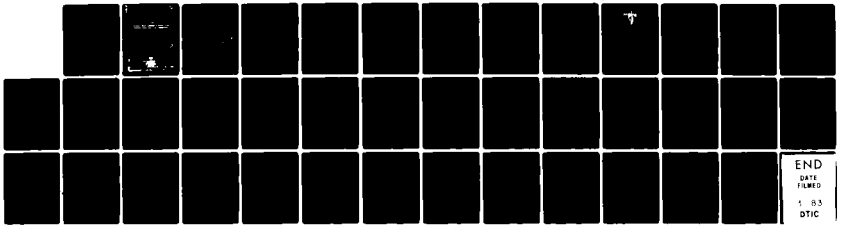

END
DATE FILMED
1 83
DTIC

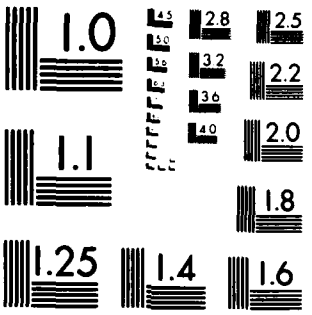

(12)

Flow Research Report No. 227

Calculation of Transonic Potential Flow Around A Wing-Body-Tail Combination

John Mercer, Wen-Huei Jou, and Margaret Johnson

April 1982

Research and Technology Division
Flow Industries, Inc.
21414-68th Avenue South
Kent, Washington 98031
(206) 872-8500

This work is supported by the Office of Naval Research under contract N00014-80-C-0453.

Unclassified

SECURITY CLASSIFICATION OF THIS PAGE (When Data Entered)

REPORT DOCUMENTATION PAGE	READ INSTRUCTIONS BEFORE COMPLETING FORM
1. REPORT NUMBER	2. GOVT ACCESSION NO. A124 247 / 3. RECIPIENT'S CATALOG NUMBER
4. TITLE (and Subtitle) Calculation of Transonic Potential Flow Around a Wing-Body-Tail Combination	5. TYPE OF REPORT & PERIOD COVERED Final 5/7/80 - 9/30/81 6. PERFORMING ORG. REPORT NUMBER FR Report No. 227
7. AUTHOR(s) John Mercer Wen-Huei Jou Margaret Johnson	8. CONTRACT OR GRANT NUMBER(s) N00014-80-C-0453
9. PERFORMING ORGANIZATION NAME AND ADDRESS Flow Industries, Inc. 21414 - 68th Avenue South Kent, WA 98032	10. PROGRAM ELEMENT, PROJECT, TASK AREA & WORK UNIT NUMBERS
11. CONTROLLING OFFICE NAME AND ADDRESS Office of Naval Research - Dept. of the Navy 800 North Quincy Street Arlington, VA 22217	12. REPORT DATE April 1982 13. NUMBER OF PAGES 33
14. MONITORING AGENCY NAME & ADDRESS(if different from Controlling Office) Defense Contract Administration Services Management Area - Seattle, Bldg. 5D, Naval Support Activity - 7500 Sand Point Way N.E. Seattle, WA 98115	15. SECURITY CLASS. (of this report) Unclassified 15a. DECLASSIFICATION/DOWNGRADING SCHEDULE

16. DISTRIBUTION STATEMENT (of this Report)

This document has been approved for public release and sale; its distribution is unlimited.

17. DISTRIBUTION STATEMENT (of the abstract entered in Block 20, if different from Report)

18. SUPPLEMENTARY NOTES

19. KEY WORDS (Continue on reverse side if necessary and identify by block number)

- transonic flow
- finite-volume method
- mesh generation

20. ABSTRACT (Continue on reverse side if necessary and identify by block number)

An embedded mesh system for transonic flow analysis is described. The method has been applied to the finite-volume potential flow calculation of flows around wing-body-tail configurations. A local C-type mesh is fitted to a horizontal tail mounted on a wing-body around which a wraparound C-type mesh has also been used. Sample calculations for a modified A-7 configuration and another wing-body-tail configuration are given. The results show rapid convergence and excellent details of pressure distribution over the entire configuration in both cases.

DD FORM 1 JAN 73 1473

Unclassified

SECURITY CLASSIFICATION OF THIS PAGE (When Data Entered)

Abstract

An embedded mesh system for transonic flow analysis is described. The method has been applied to the finite-volume potential flow calculation of flows around wing-body-tail configurations. A local C-type mesh is fitted to a horizontal tail mounted on a wing-body around which a wraparound C-type mesh has also been used. Sample calculations for a modified A-7 configuration and another wing-body-tail configuration are given. The results show rapid convergence and excellent details of pressure distribution over the entire configuration in both cases.

Table of Contents

List of Figures

1. Introduction

The finite-volume algorithm for calculating transonic potential flow around an arbitrary geometry was orginally developed by Jameson and Caughey (1977). This method is now used as the base for computational codes that analyze the flow around realistic aircraft configurations. One of the most popular of these codes is the FLO-30 code, originally developed by Flow Research Company in cooperation with Professors Jameson and Caughey (Mercer et al., 1980), which uses a C-type mesh system. The finite-volume algorithm is so flexible, however, that other equally effective and more flexible codes can be constructed using other types of mesh systems. For example, the WBT code has been developed by Flow Research Company for Arnold Engineering Development Center for simulating transonic flow around a wing-body combination in a wind tunnel. This code has been used to model the effects of arbitrary wall boundary conditions on wind tunnel models. Good agreement can be seen between results from the WBT code, using a constant pressure condition at the distant wall, and FLO-30. This agreement verifies that the finite-volume algorithm can be used on a wide variety of grid systems.

It is now possible to add other components of an aircraft to these basic wing-body codes to enhance their capabilities. In the present work, a horizontal tail is incorporated in the basic configuration. Horizontal tails with substantial lifting force can couple fairly strongly with the flow around the wing, particularly when the wing and tail are closely coupled as in many military aircraft.

In this report, the mesh generation scheme for our wing-body-tail combination is described. We show that if the C-type mesh is required around the horizontal tail to resolve the leading-edge pressure detail, it is topologically impossible to generate a unified mesh system that includes both wing and tail; an embedded mesh must be used for the horizontal tail. The solution is then obtained through interactive iterations between the main wing-body calculations and the tail calculations. Examples of these calculations are presented.

2. Mesh Generation

The existing wing-body codes, such as FLO-30 and WBT, use a C-type mesh system around the wing. The wraparound mesh lines are carried to the downstream infinity. If a wraparound C-type mesh is required for the tail region, these two families of C-type curves will be compatible downstream of the tail but incompatible in the space behind the wing and in front of the tail. This means that a single mesh that simultaneously wraps around the wing and the tail cannot be generated. Therefore, two mesh systems must be employed, one for the wing and one for the horizontal tail, and the tail system must be embedded into the wing system. As a means of defining the outer boundary of the tail region, a set of grid lines from the wing grid system is used as shown in Figure 1. This procedure creates two computational modules: a wing-body calculation and a tail calculation. The boundary of the wing-body calculation extends into the interior of the tail region. This overlapping of the two grids allows for the transfer of information between the two calculations as discussed in Section 3.

2.1 Wing-Body Mesh

The WBT code developed for a wing-body combination in a wind tunnel was chosen in favor of the FLO-30 code as the basic code for incorporation of a horizontal tail. There are several reasons for this choice. The FLO-30 code uses a cylindrical-type mesh which has "spanwise" coordinate surfaces wrapped around the fuselage. This system makes it very difficult to model tail configurations which lie near or off the edge of the fuselage, such as is often the case. Also, the vortex wake trajectory from the wing becomes difficult to model with the cylindrical-type mesh. This is due to the fact that the wake must lie on a grid surface and so must be displaced to a boundary of the tail mesh. In general, the wake cannot pass through the tail since there is no mesh line in a C-type mesh that goes from the upstream boundary to the downstream boundary (except the one which passes through the tail). If the vortex wake is distorted to the tail region boundary on a cylindrical-type mesh, the wake will not only be displaced vertically but also horizontally. The horizontal displacement can produce large errors for the downwash effect on the horizontal tail. The WBT code uses a mesh system that results from transforming the fuselage cross sections to a vertical slit. The horizontal tail is easily modeled as a tail on a wall in the transformed space whether it is on the fuselage or not. Also a spanwise

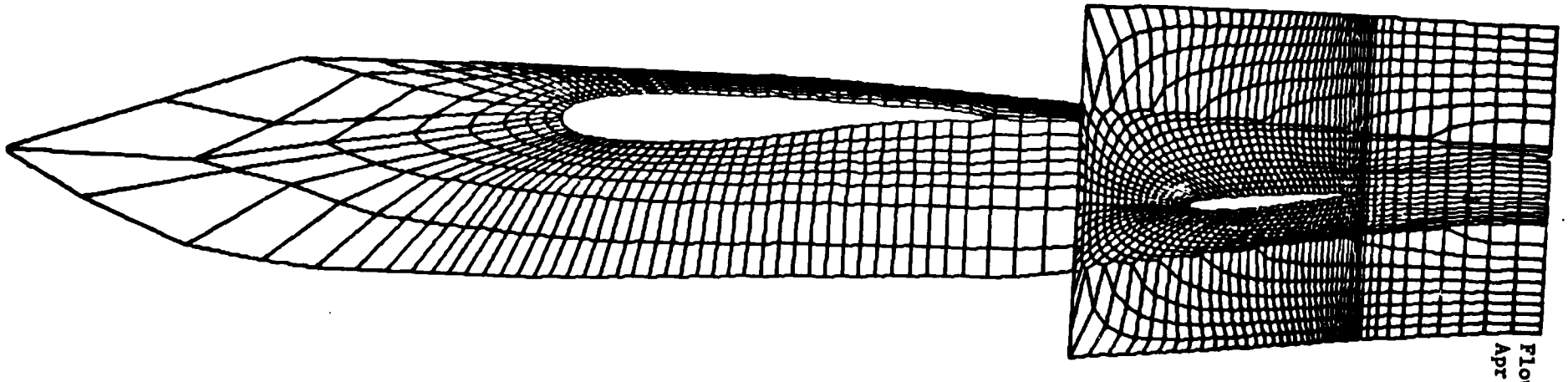

Figure 1. Embedded Tail Mesh

station is roughly a spanwise slice. The displacement of the wing vortex wake in the spanwise plane moves the vortex wake upward without significantly changing the spanwise location. Lastly, a code that can be used for both free-air calculations and wind tunnel simulations will be extremely valuable both as a design tool and as a tool to assess wind tunnel test results.

The procedure for generating a wing-body mesh in the WBT code can be summarized as follows:

(1) The first step is to transform a series of circular cross sections, with centers and radii determined by the height and location of the fuselage cross sections, to vertical slits by use of the well-known Joukowsky transformation. Under this transformation, a noncircular fuselage will become a distorted slit.

(2) Next, a shearing transformation in the spanwise direction is used to remove this distortion of the fuselage.

(3) The computational domain in this Joukowsky-shear transformed space is then sliced into spanwise sheets on which the wraparound C-type mesh will be generated.

(4) On the spanwise station wrapping around the fuselage, two boundaries must be placed on mesh lines: one is the intersection of the fuselage with the wing root, and the other is the upper and lower edges of the fuselage that has been transformed to a slit. Both of these boundaries must be mesh lines of the wraparound family. To be consistent with the topology of the fuselage station just described, images of the "fuselage" are defined for the other spanwise stations. These images are defined so that the mesh system continuously varies from the fuselage shape at the innermost station to an open-elliptical shape at the tip station and beyond.

(5) For wind tunnel applications, an additional boundary is required. This is a rectangular boundary at the outer limit of the computational domain corresponding to the tunnel wall. For free-air calculations, this boundary is assumed to be a large distance away from the configuration.

(6) It is not possible to generate a family of C-type curves, including three known curves, with a conformal transformation. Thus, the application of the mesh generation scheme using an elliptic equation is ruled out when it is compared to the following simple, algebraic, mesh generation scheme.

A family of "superellipses" is generated by the following formula:

$$\left(\frac{x}{a}\right)^m + \left(\frac{y}{b}\right)^m = 1 \qquad (1)$$

where the parameter a is the semi-major axis, b is the semi-minor axis, and m controls the curvature of the superellipse. For example, as m approaches infinity, the superellipse approaches a rectangle. The family of superellipses used in this work is characterized by the following properties:

(a) The parameter b varies from the half-thickness of the wing at the innermost curve, to the maximum half-height of the "fuselage" image at a designated mesh index, and to the "tunnel" half-height at the outer boundary.

(b) The semi-major axis, a, varies from the chord length of the wing, to the distance between the nose of the fuselage and the trailing edge of the wing at a designated mesh index, and to the distance between the upstream boundary and the trailing-edge boundary.

(c) The parameter m varies from 2 at the innermost ellipse to infinity at the outer boundary.

(d) The trailing edge of the wing is defined as the origin of the family of superellipses.

This process generates a family of curves of which three members have approximate thickness ratios of the wing, the fuselage, and the tunnel wall (outer boundary), respectively. These C-type curves are continued horizontally from the trailing edge to the downstream boundary.

(7) To form a computational mesh, these C-type curves must be intersected by another family of curves. The innermost curve is

divided into segments so that the segments are small near the leading edge. The outer boundary is also divided into an equal number of segments. Starting from the upstream point, the corresponding points on these two curves are connected by straight lines. The intersections between the straight lines and the C-type curves are computed. These intersections define a mesh network.

(8) The next task in the mesh generation is to make it a body-fitted mesh. This is accomplished by shearing the mesh vertically so that the innermost C-type curve is moved to the actual wing profile and the C-type curve designated as the fuselage mesh line is moved to the actual fuselage image.

(9) Finally, these two-dimensional meshes are transformed to the physical space by an inverse Joukowsky-shearing transformation.

This procedure for generating a wing-body mesh is demonstrated schematically in Figure 2.

This mesh generation scheme has a number of advantages over the FLO-30 scheme. First of all, the scheme can be used for free-air calculations as well as wind tunnel simulations, when the latter are required. Second, the extension of the mesh upstream is an input parameter, which insures that the upstream boundary conditions are applied at a distance sufficiently upstream. It has been observed that the FLO-30 mesh, particularly that portion near the fuselage, does not extend very far upstream. This has caused some problems in the accuracy of the application of the far-field free-stream conditions.

2.2 Tail Mesh

In the Joukowsky-sheared space of the wing-body mesh, a region in the neighborhood of the tail is cut out. This region is defined by a vertical line in the wing-body mesh a certain distance upstream of the leading edge of the tail and by two horizontal mesh lines. The upper and lower boundaries of the tail region must be defined sufficiently far away from the tail so that the supersonic bubble generated by the tail does not cross the boundaries. Due to the disparity in the mesh spacings between the wing-body mesh and the tail mesh on these boundaries, interpolation of the velocity potential there can cause errors in the mass conservation formula. This can

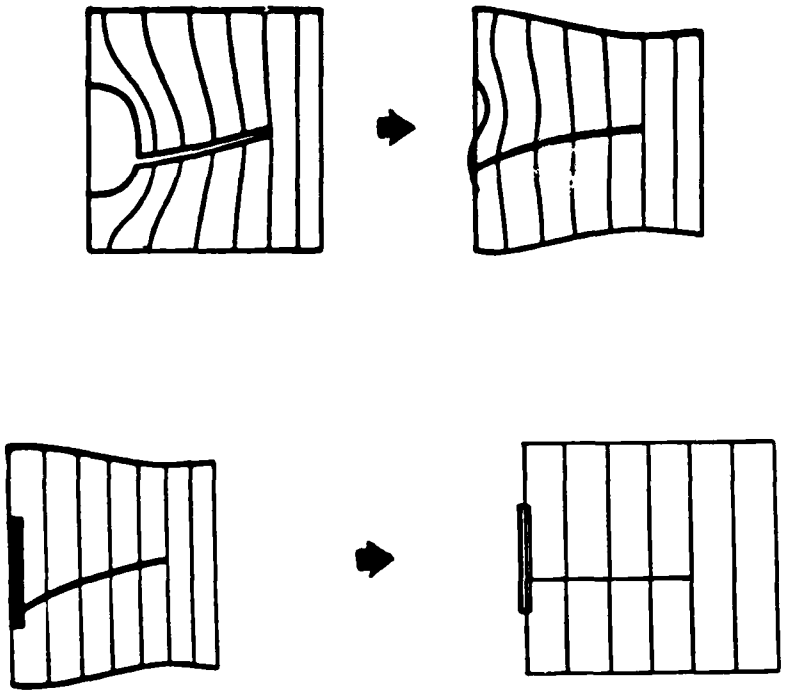

- Generate 2-D Mesh on Spanwise Stations

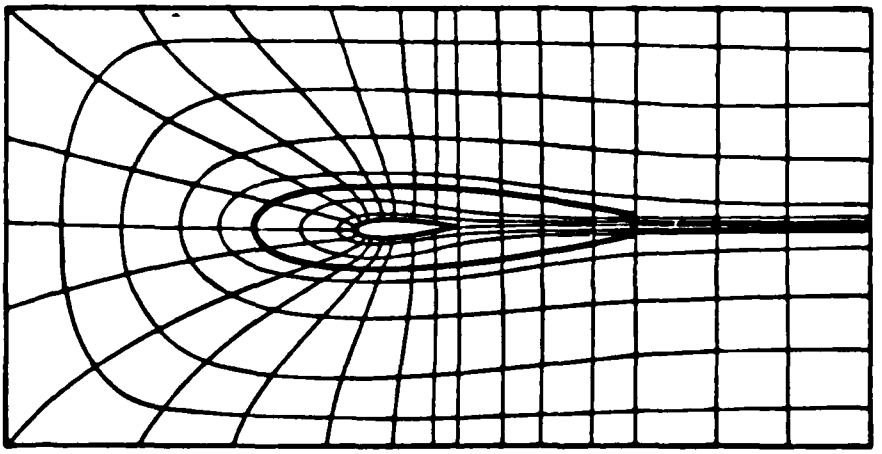

- Use Super-Ellipses

Figure 2. Mesh Generation Procedure

be a severe problem in the supersonic region. The present choice of the outer boundary above and below the fuselage image will create some "fin" effects (see Mercer et al., 1980). However, the tail mesh is sufficiently dense so that the fin effects are not pronounced.

The tail mesh is generated in essentially the same way as the wing-body mesh, except that the fuselage image is ignored and the outer boundary is that given by the wing-body mesh.

For a modified A-7 airplane, the side view of the combined wing-body and tail meshes on the "fuselage" spanwise station is shown in Figure 1. For the purpose of clarity, the wing-body mesh outside of the fuselage image is not plotted. The fuselage in the tail region shows some small "fins" on its top and bottom.

3. Numerical Calculations

The calculation of the velocity potential is carried out by using the finite-volume method with the following strategy of interactive computations:

(1) The wing-body calculation is performed with a region of the tail cut out. The boundary points at the interface extend one mesh line into the tail domain. The potential values on the boundary points are obtained by interpolation from the interior points of the tail computations.

(2) During the wing-body calculations, the circulation around the wing section continuously increases with each iteration. The change in circulation after each iteration is divided between the upper and lower boundaries around the tail region and is added or subtracted from the potential values on the boundary points.

(3) After a few iterations, the computational mode is switched to the tail calculation. The potential at the boundary points in the interior of the wing-body domain is obtained by interpolation from the wing-body calculations, with the proper potential jump subtracted from the potential on those points located above the vortex wake. This operation equivalently places the wing vortex wake on the upper boundary of the tail region. The downwash and the averaged spanwise flow induced by the wing are fairly well approximated by this method. Only the velocity shear on the vortex wake is at the displaced location.

(4) After a few iterations in the tail computation, the potential on the boundary points of the wing-body mesh is obtained through interpolation with the proper potential jump added.

(5) The process is repeated until convergence.

The code is written for use in a computer with virtual memory or a large-core computer such as the Cray 1.

A general "field-point interrogator" is programmed to interpolate the velocity potential at the boundary. This interrogator essentially treats the transformation from the physical space (x, y, z) to the transformed space (i, j, k) as a nonlinear function. Given a set of arbitrary physical coordinates (x_0, y_0, z_0), one can treat the (i, j, k) space as a continuous space and locate a noninteger location (i_0, j_0, k_0) in the computational

space by use of Newton's method. The velocity potential at that point can be obtained from that at the surrounding mesh points using the trilinear formula. This interrogator makes the transfer of information at the interfacial boundary extremely simple.

4. Results

The code described in the previous sections has been applied to a modified A-7 aircraft with a high wing position. The tail is modeled as a 7.5-percent symmetric NACA 00075 airfoil with a -6 degree angle of incidence relative to the defining coordinate axis. The planforms of the wing and the tail with their frontal views are given in Figure 3.

The computed pressure distributions on the wing and the tail are displayed in Figures 4 through 12. For a free-stream Mach number of 0.85 and an angle of attack at 4.68 degrees, the pressure distribution on the tail does not show any shock wave effects. Near the trailing edge of some of the wing sections, however, a dip in the pressure plots can be seen. Careful examination of the given data shows that a concave kink is present on the upper surface of the airfoil near the trailing edge. No attempt has been made to smooth the kink and possibly improve the appearance of the pressure plot.

The code was also applied to a wing-body geometry given by SAAB of Sweden. The configuration has a high wing geometry with a cylindrical body, and a horizontal tail has been added. The tail is a NACA 0005 airfoil at a zero degree angle relative to the defining coordinate. The planforms of the wing and the tail together with their frontal views are given in Figure 13. The pressure distributions on the wing and the tail are given in Figures 14 through 22.

The iterative process in the code is organized into outer wing-tail interactive iteration loops and inner iterations. We found that good convergence can be achieved with five inner iterations for both wing-body calculations and tail calculations. Since the convergence is fairly rapid, the total number of iterations, i.e., the number of outer iterations multiplied by the number of inner iterations, is comparable to the wing-body code.

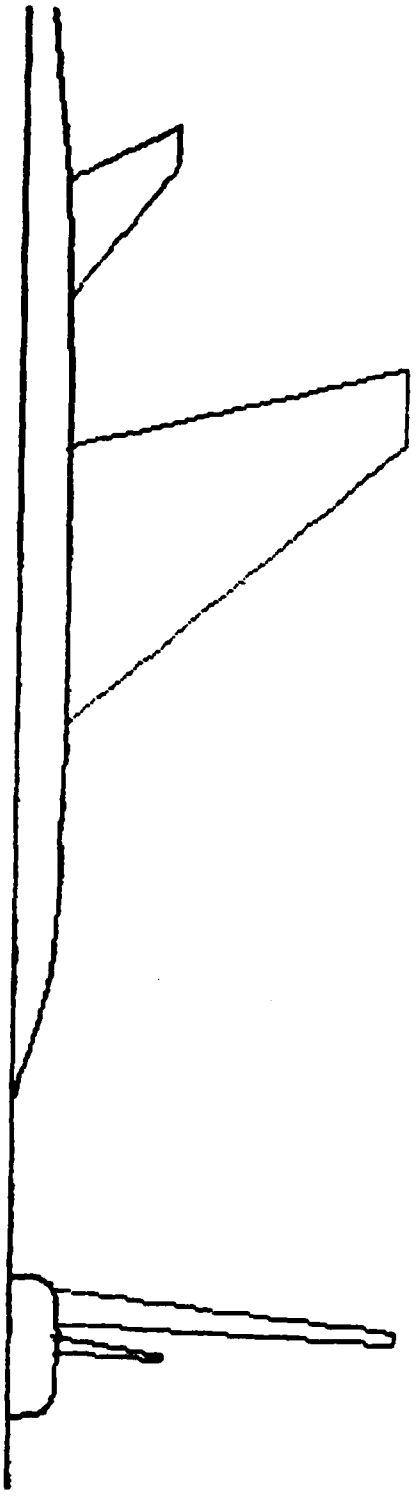

Figure 3. Wing and Tail Planforms for A-7

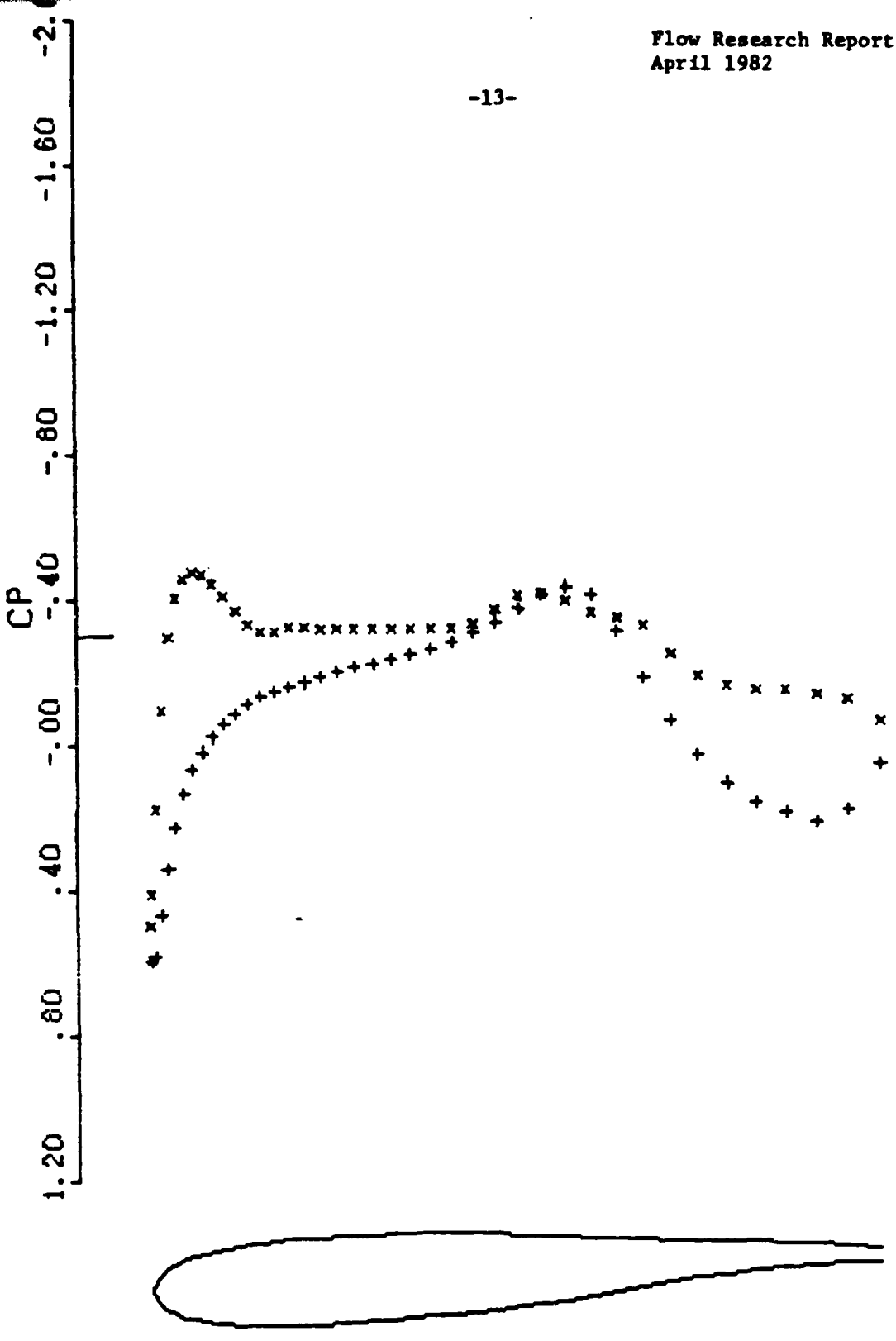

Figure 4. A-7 Wing Pressure

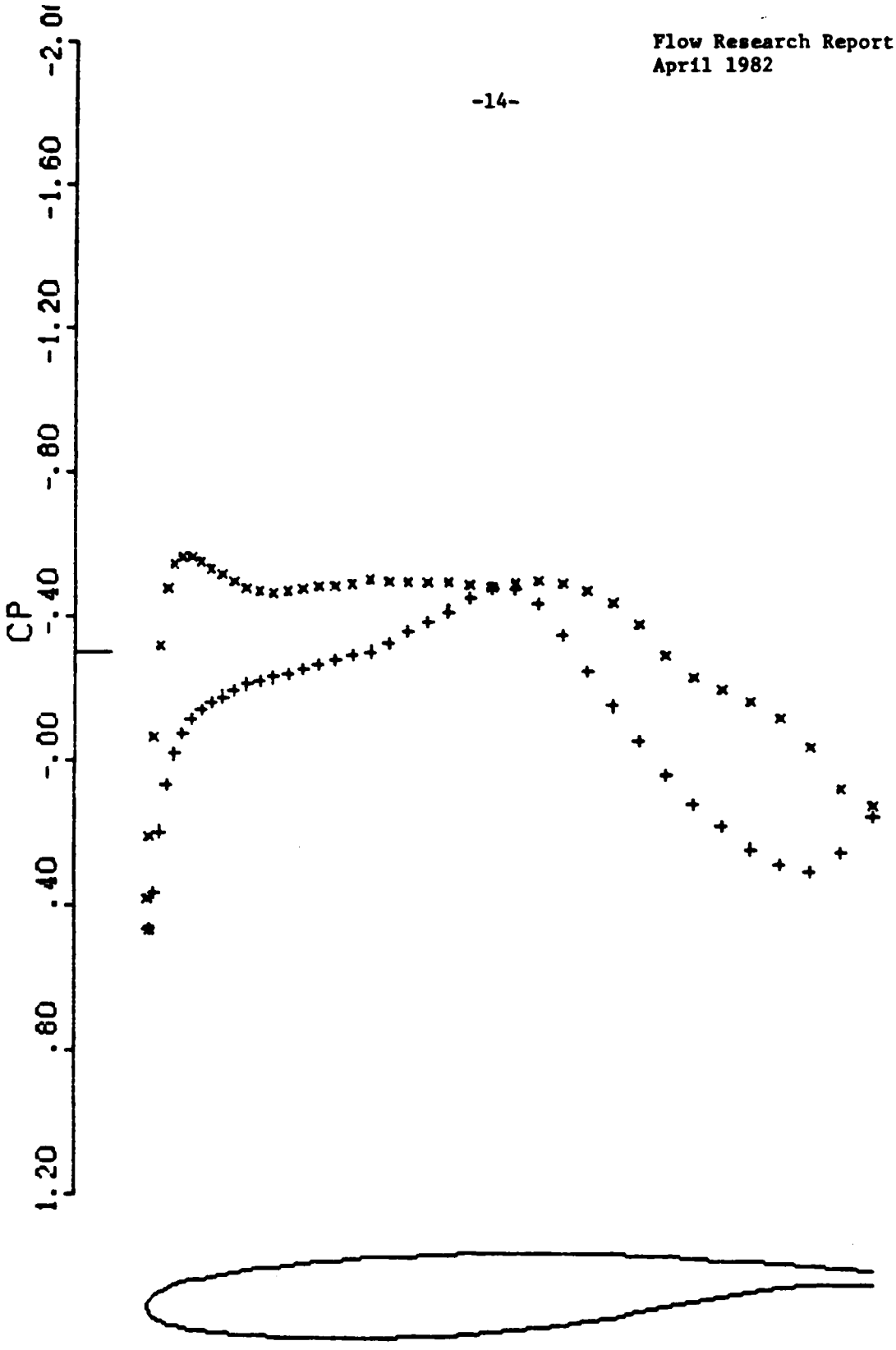

A-7 TRSON WING W2 W/B FUS F1B WING AT Y=120.
MACH 0.850 ALPHA 4.680
Z 81.40 CL 0.2437 CD 0.0102

Figure 5. A-7 Wing Pressure

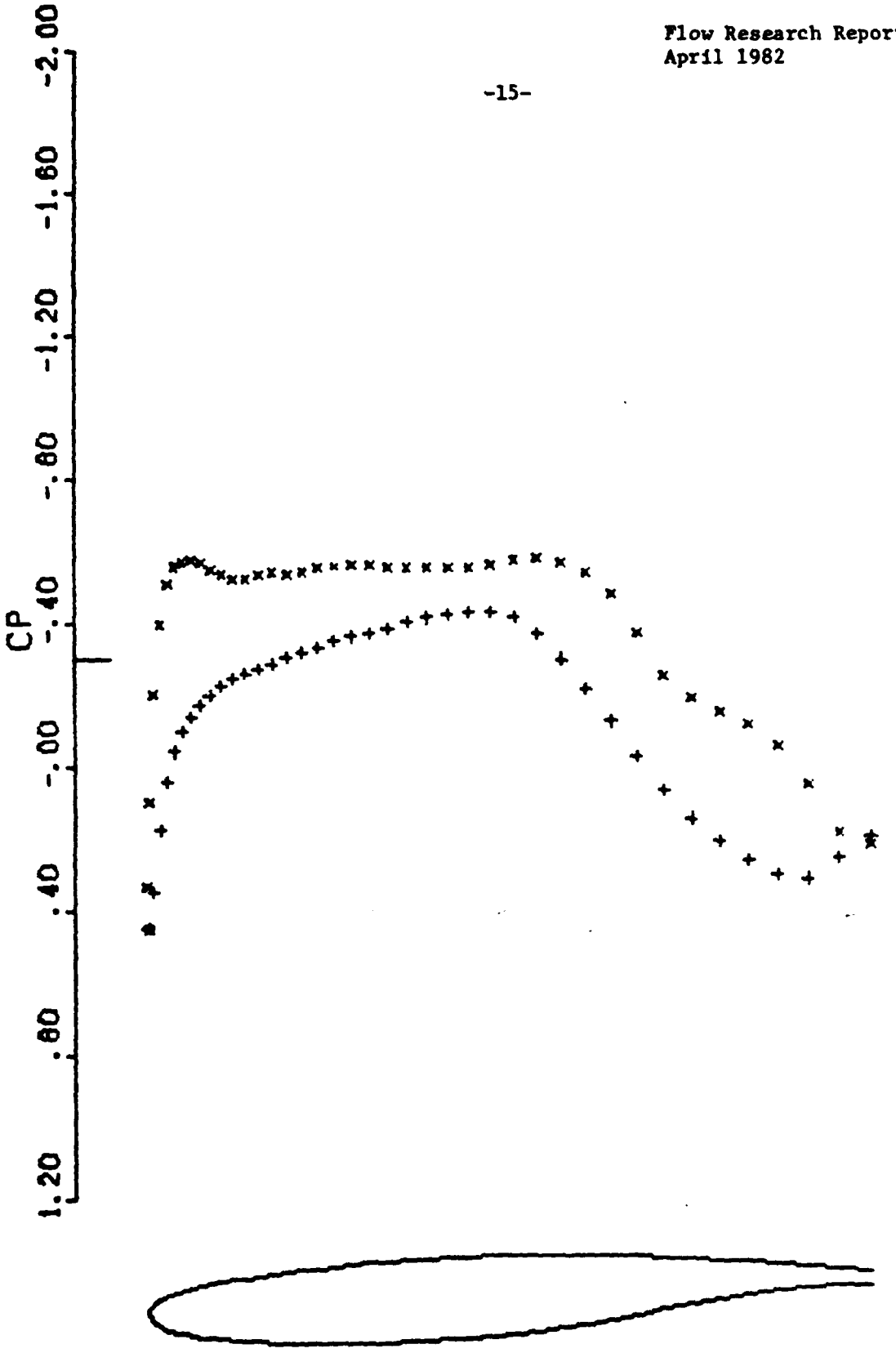

A-7 TRSON WING W2 W/B FUS F1B WING AT Y=120.
MACH 0.850 ALPHA 4.680
Z 136.60 CL 0.2612 CD -0.0011

Figure 6. A-7 Wing Pressure

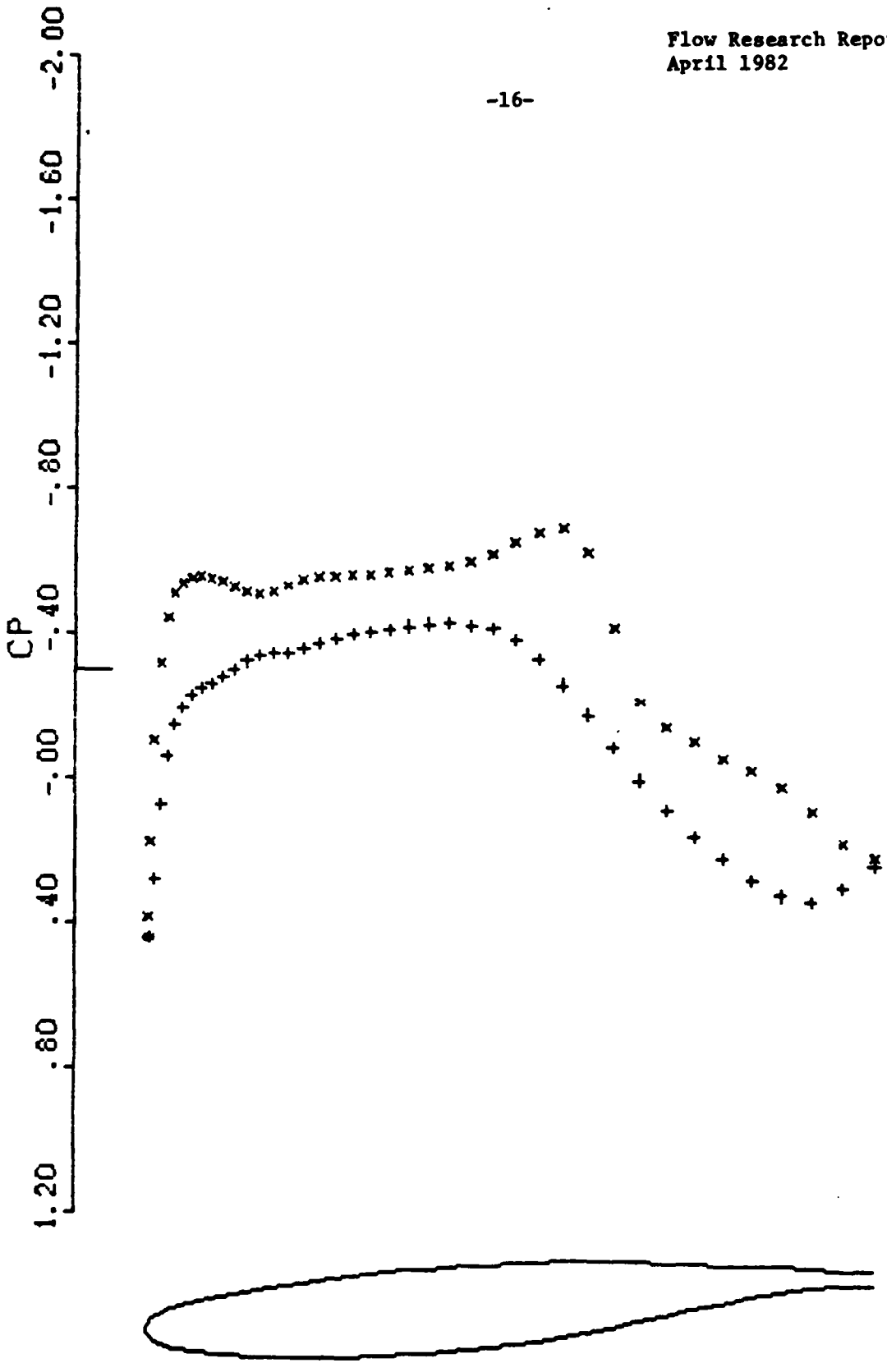

Figure 7. A-7 Wing Pressure

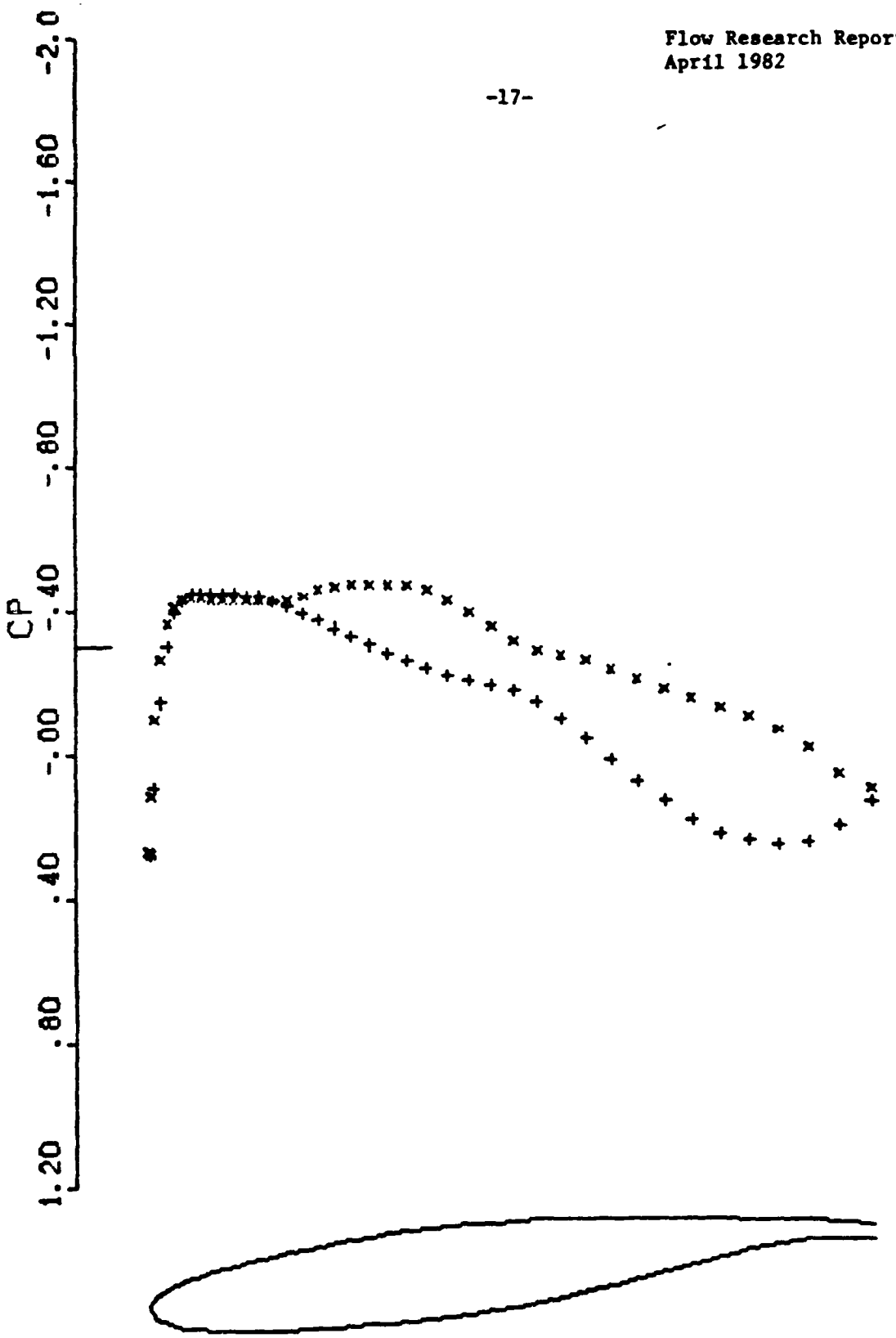

A-7 TRSON WING W2 W/B FUS F1B WING AT Y=120.
MACH 0.650 ALPHA 4.680
Z 232.98 CL 0.1781 CD -0.0287

Figure 8. A-7 Wing Pressure

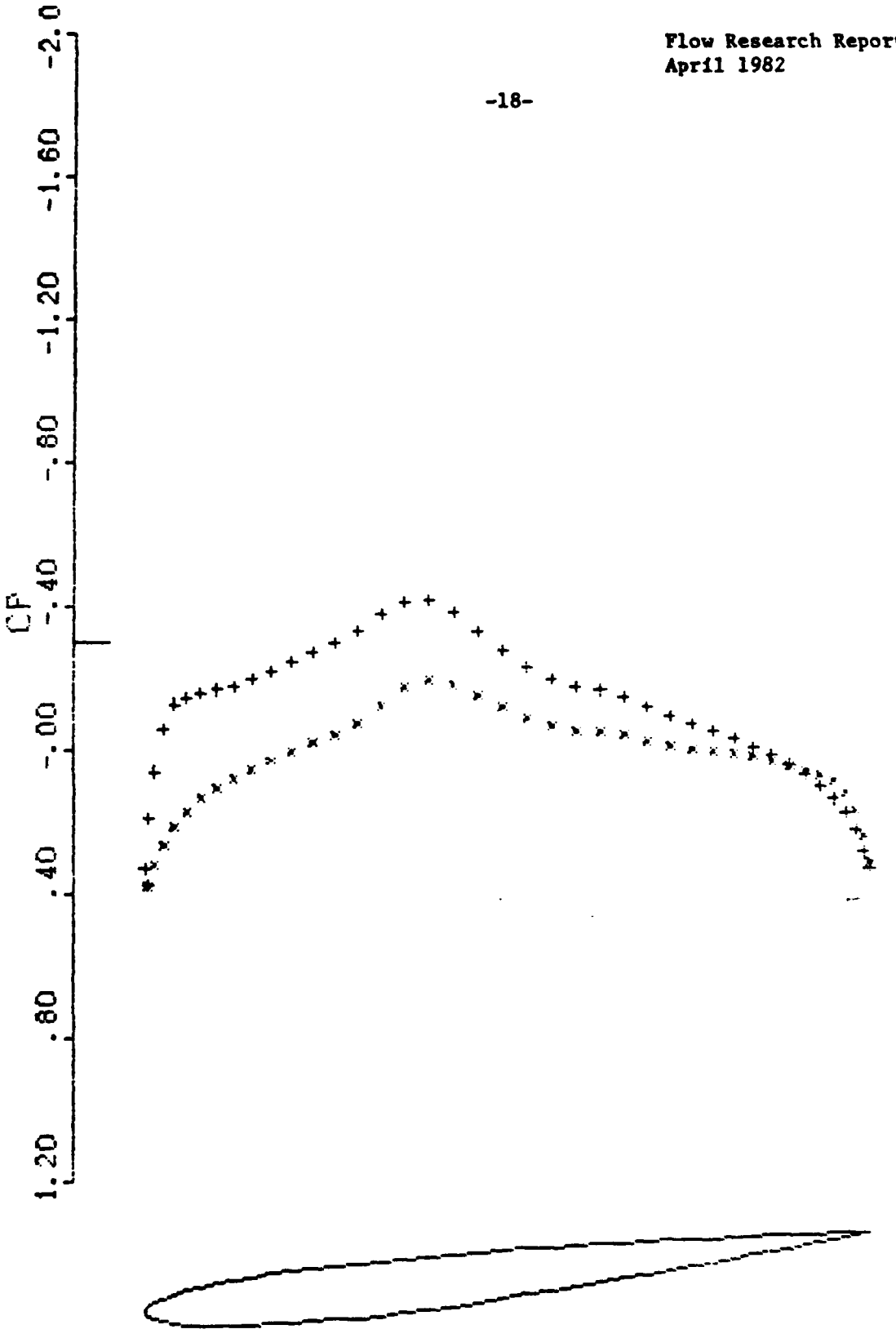

Figure 9. A-7 Tail Pressure

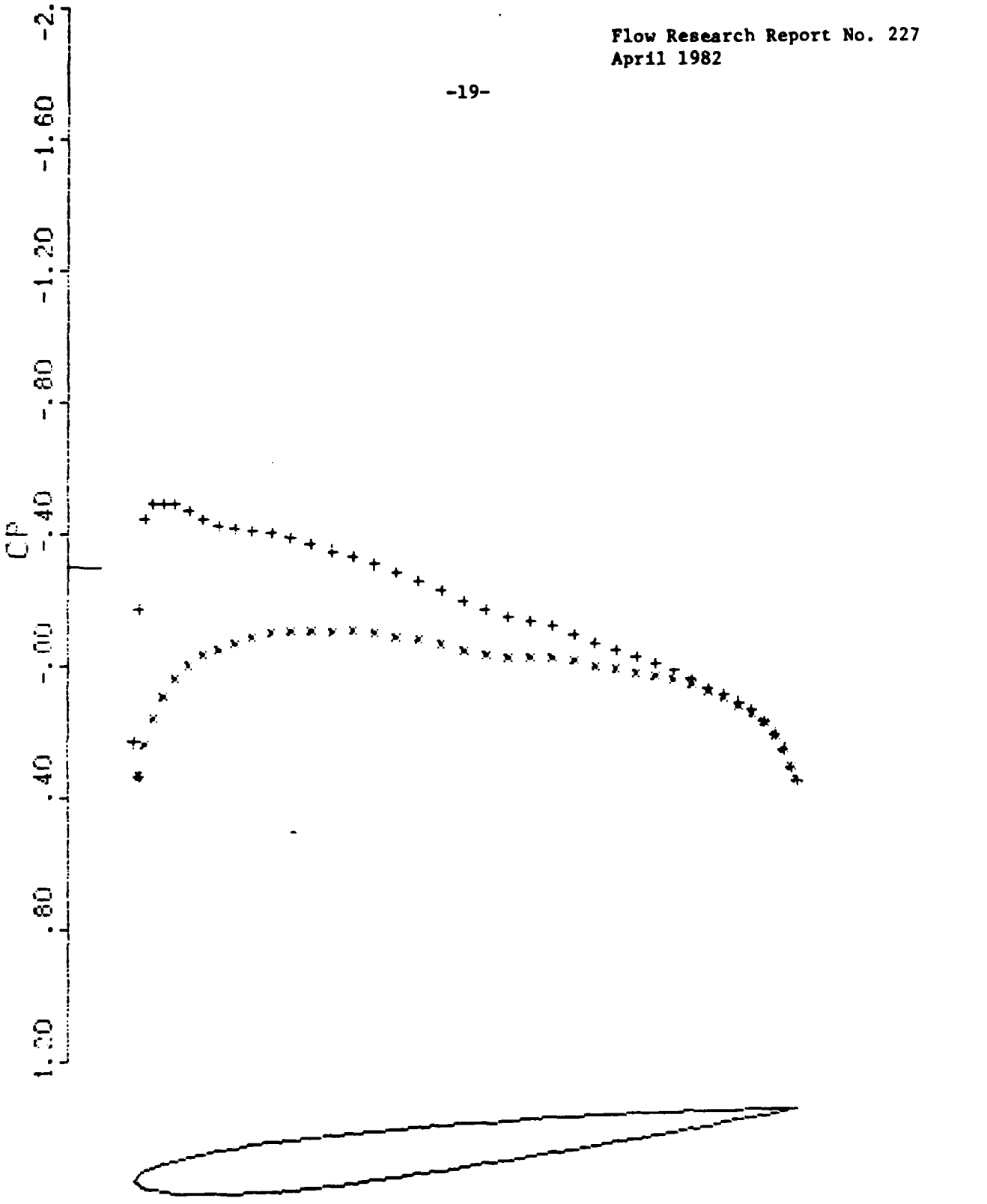

Figure 10. A-7 Tail Pressure

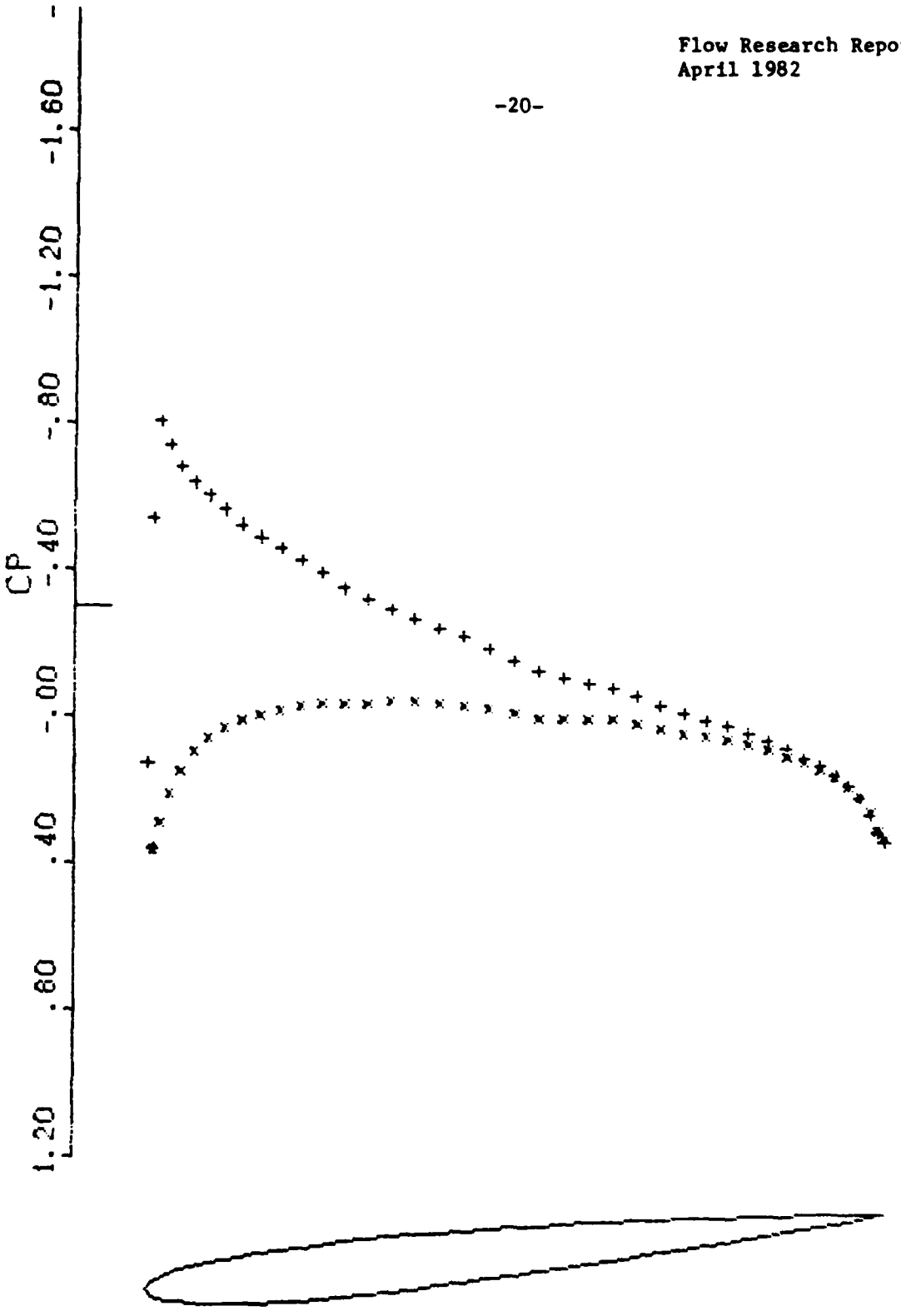

A-7 TRSON WING W2 W/B FUS F1B WING AT Y=120.
MACH 0.850 ALPHA 4.680
Z 74.16 CL -0.2295 CD -0.0105

Figure 11. A-7 Tail Pressure

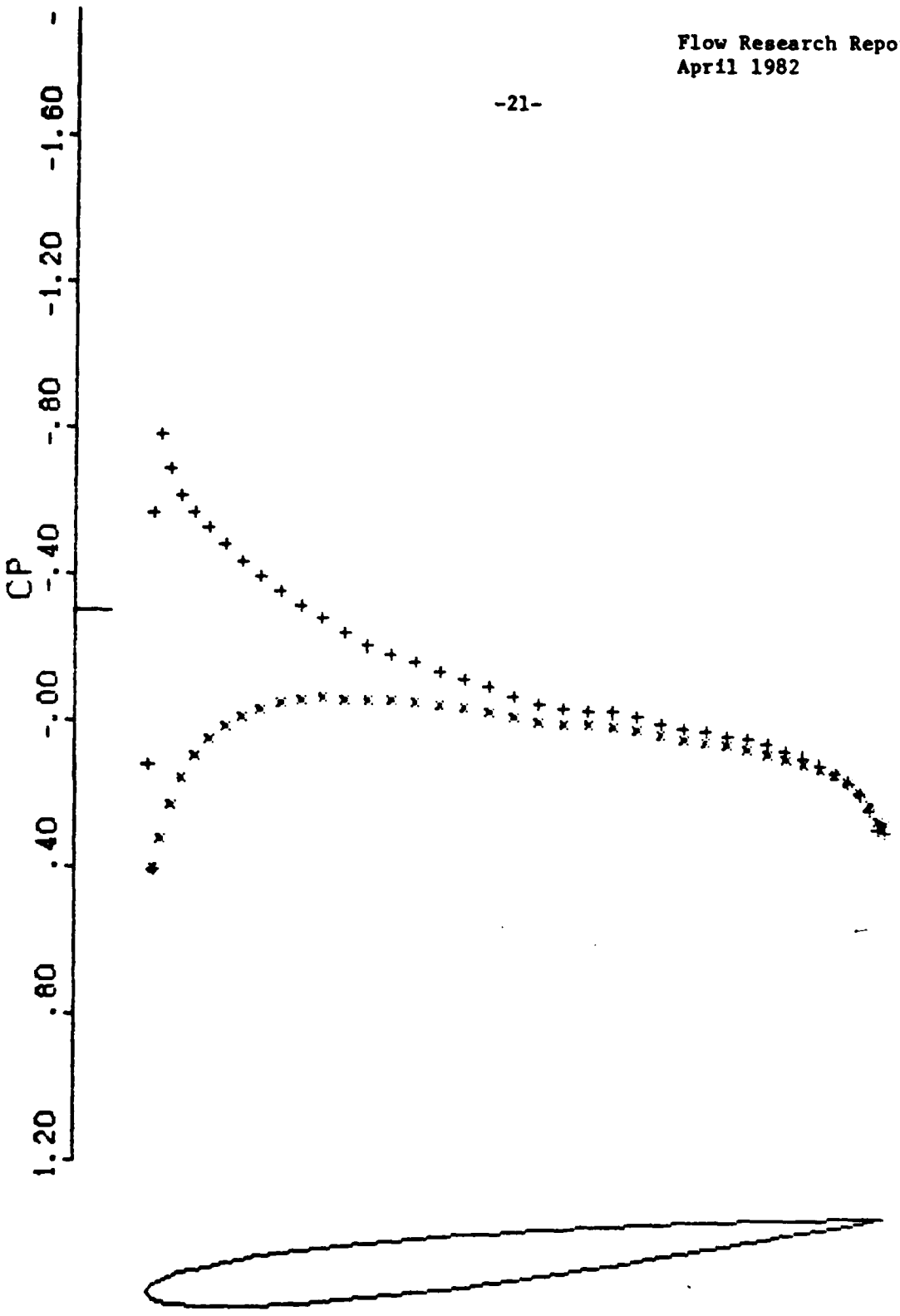

A-7 TRSON WING W2 W/B FUS F1B WING AT Y=120.
MACH 0.850 ALPHA 4.680
Z 93.00 CL -0.1634 CD -0.0122

Figure 12. A-7 Tail Pressure

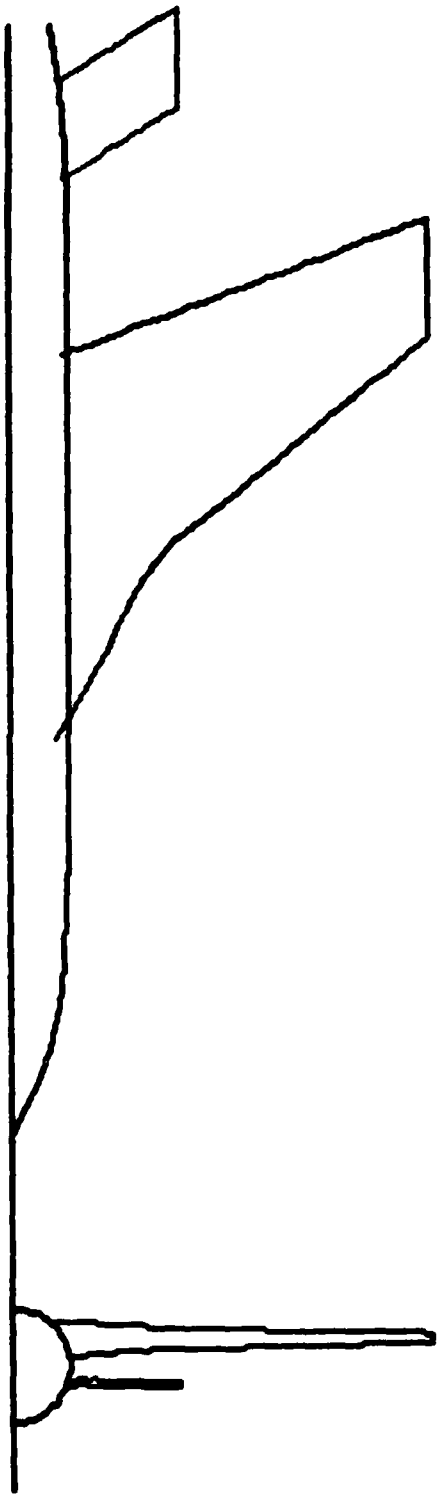

Figure 13. SAAB Wing and Tail Planforms

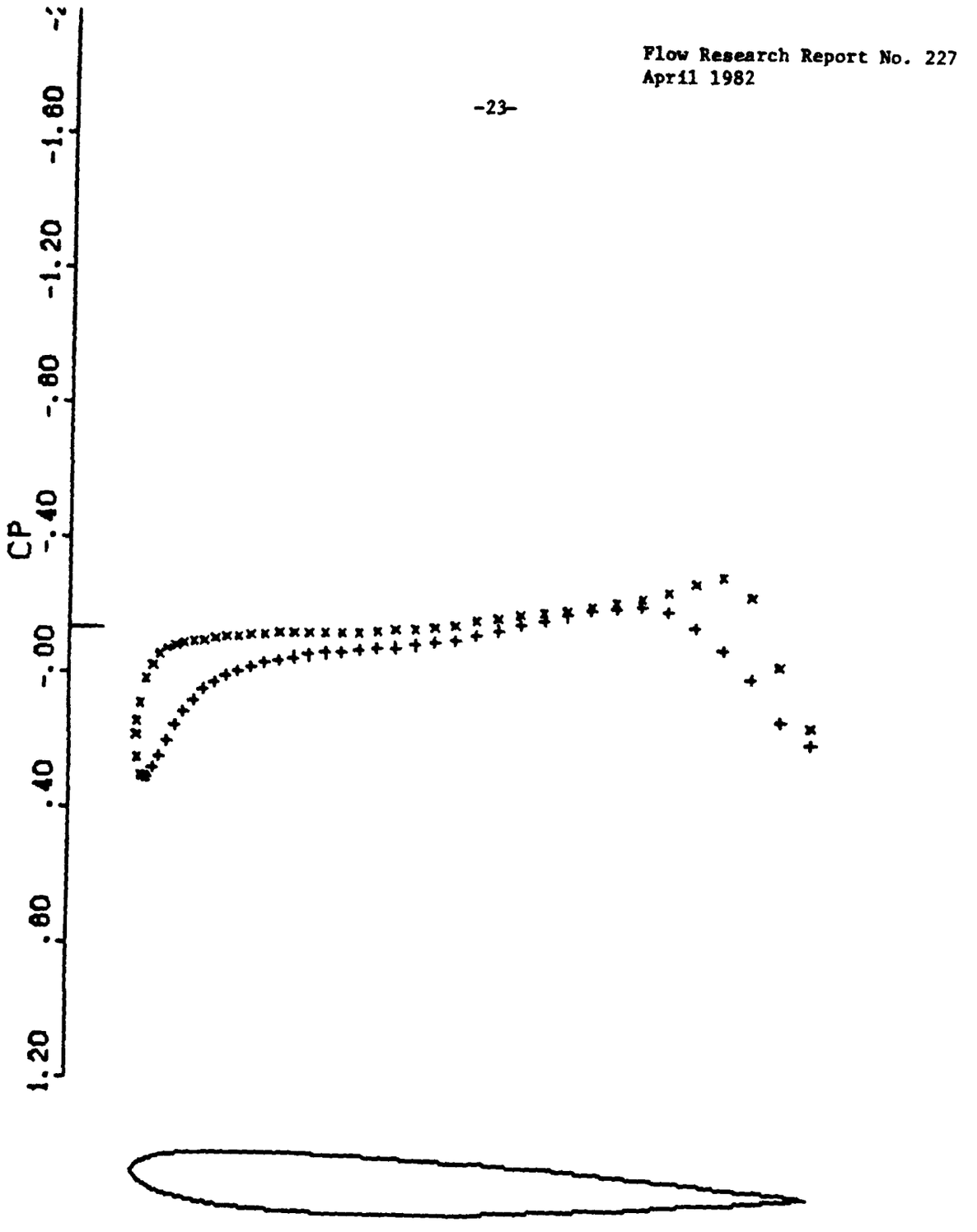

Figure 14. SAAB Wing Pressure

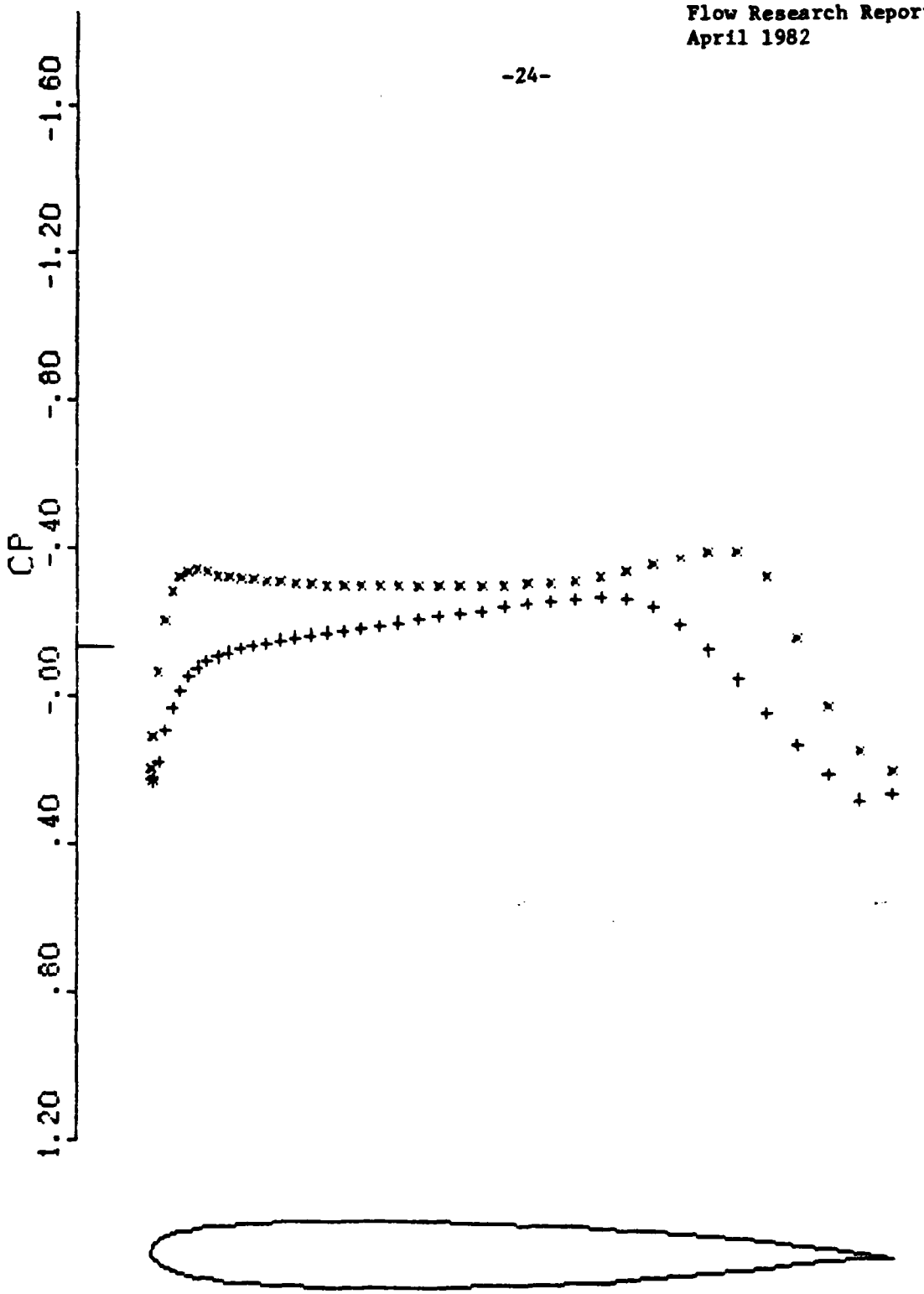

WINGBODY - TRANSONISK VINGE - SAAB-CYL (TWT)
MACH 0.925 ALPHA 1.000
Z 1.52 CL 0.1569 CD 0.0114

Figure 15. SAAB Wing Pressure

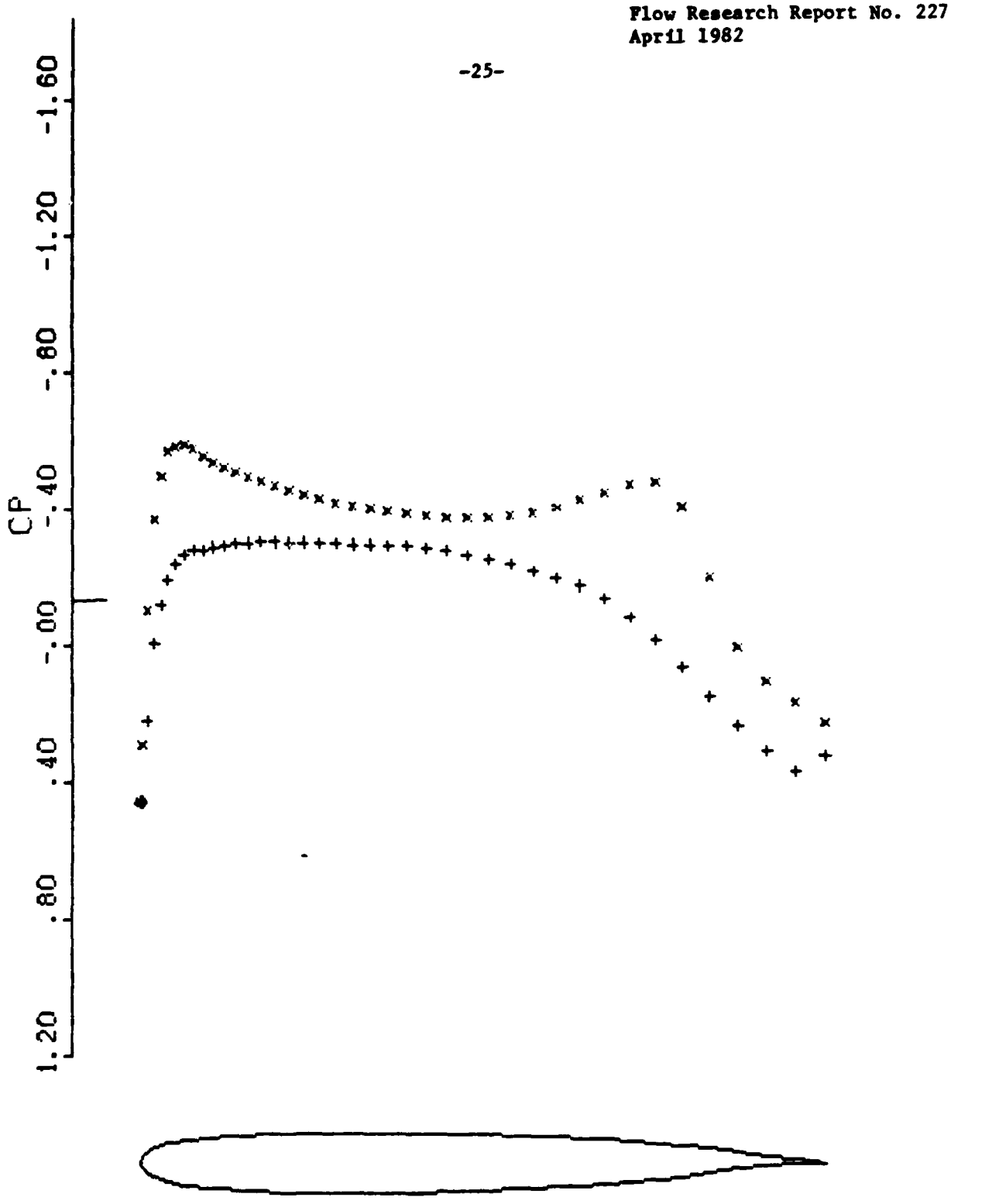

Figure 16. SAAB Wing Pressure

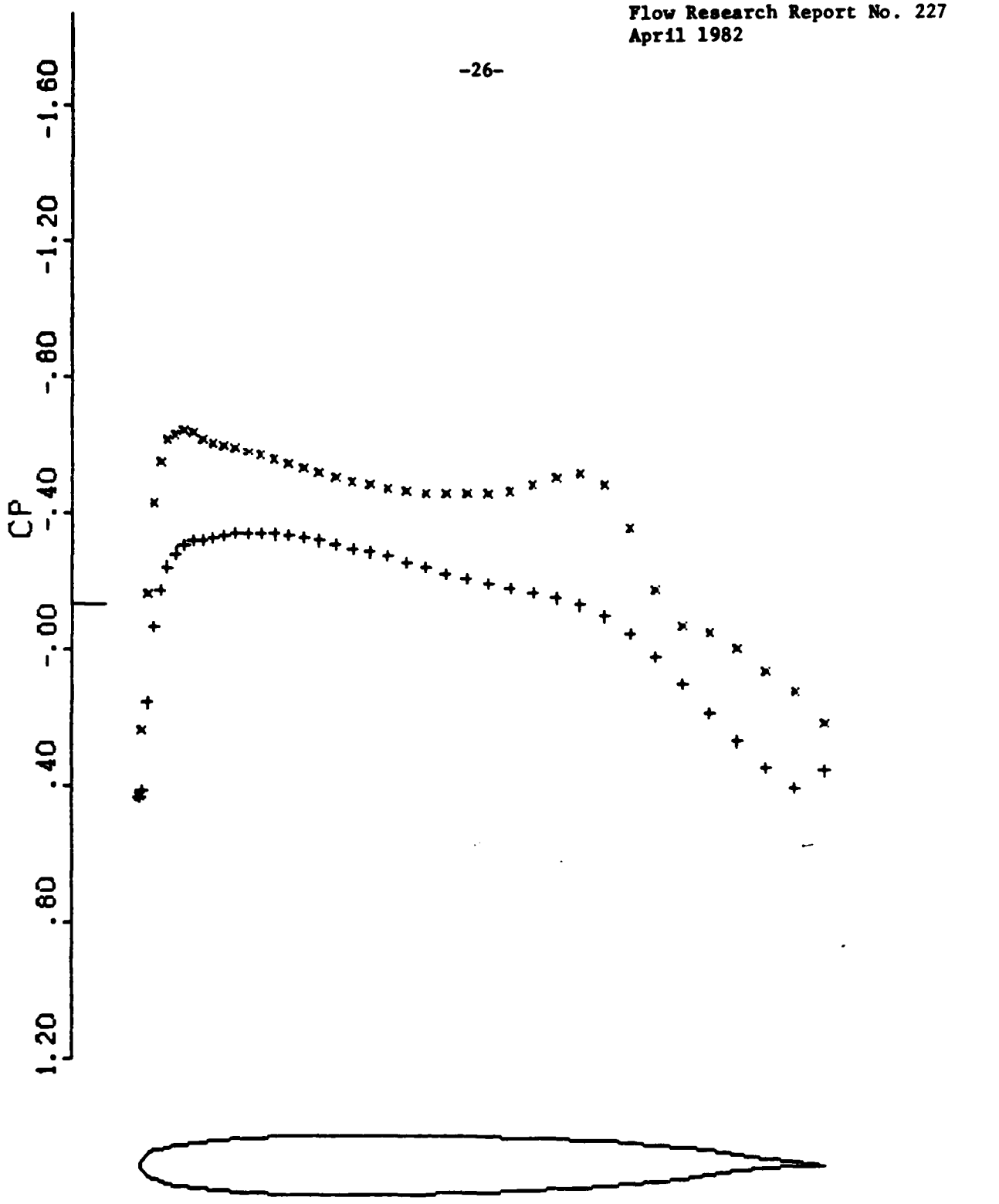

Figure 17. SAAB Wing Pressure

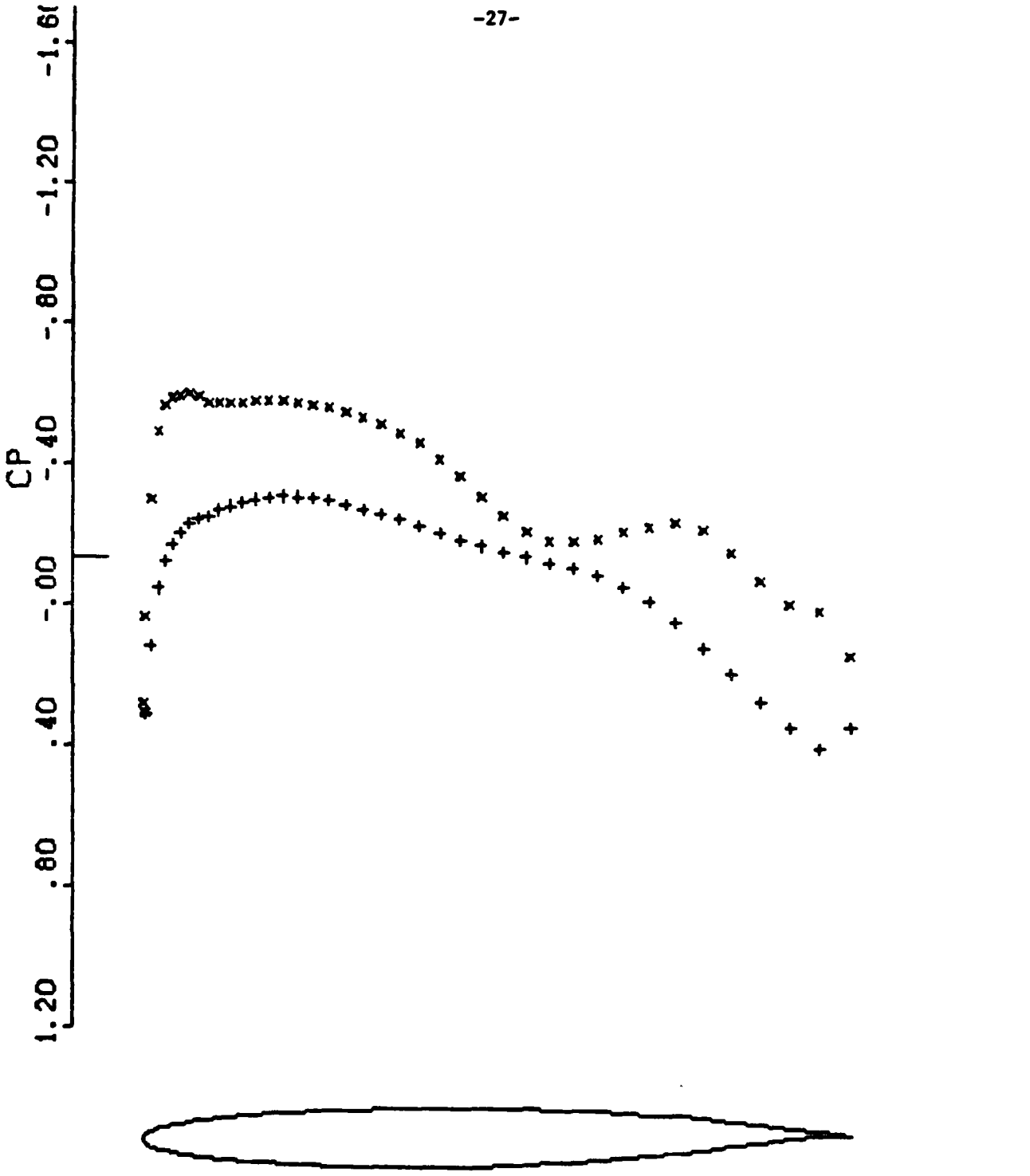

Figure 18. SAAB Wing Pressure

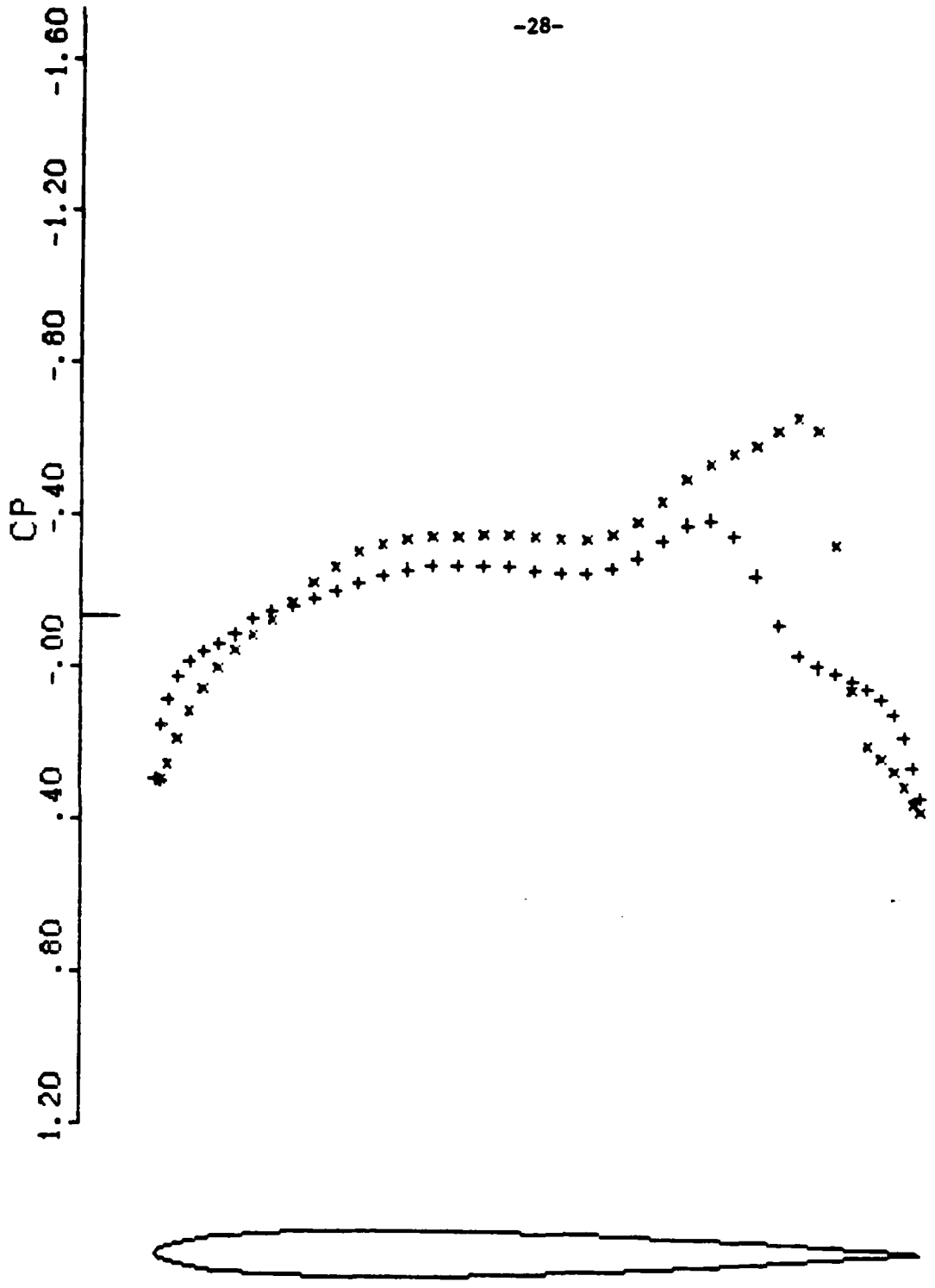

Figure 19. SAAB Tail Pressure

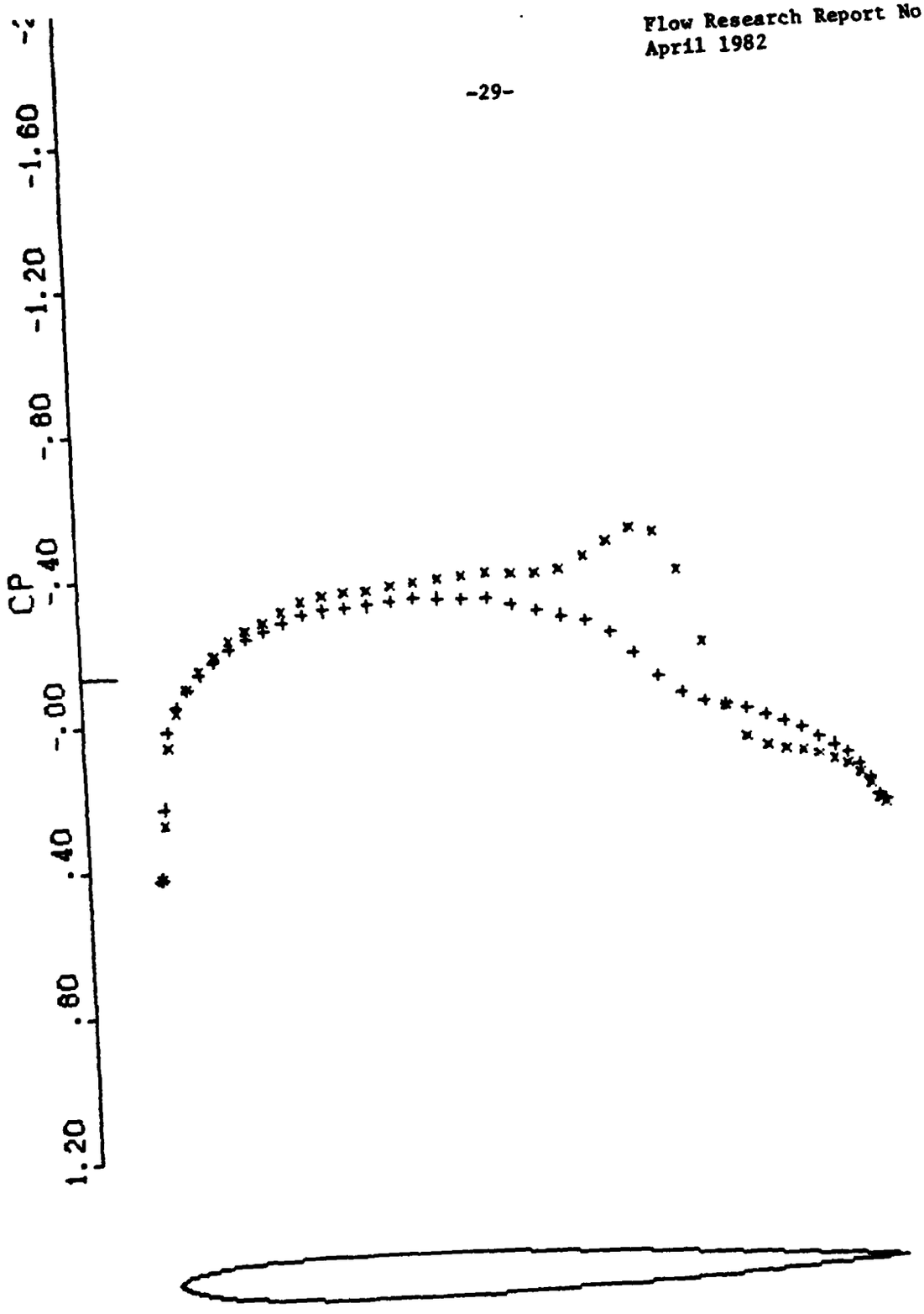

WINGBODY - TRANSONISK VINGE - SAAB-CYL (TWT)
MACH 0.925 ALPHA 1.000
Z 0.98 CL 0.0687 CD 0.0067

Figure 20. SAAB Tail Pressure

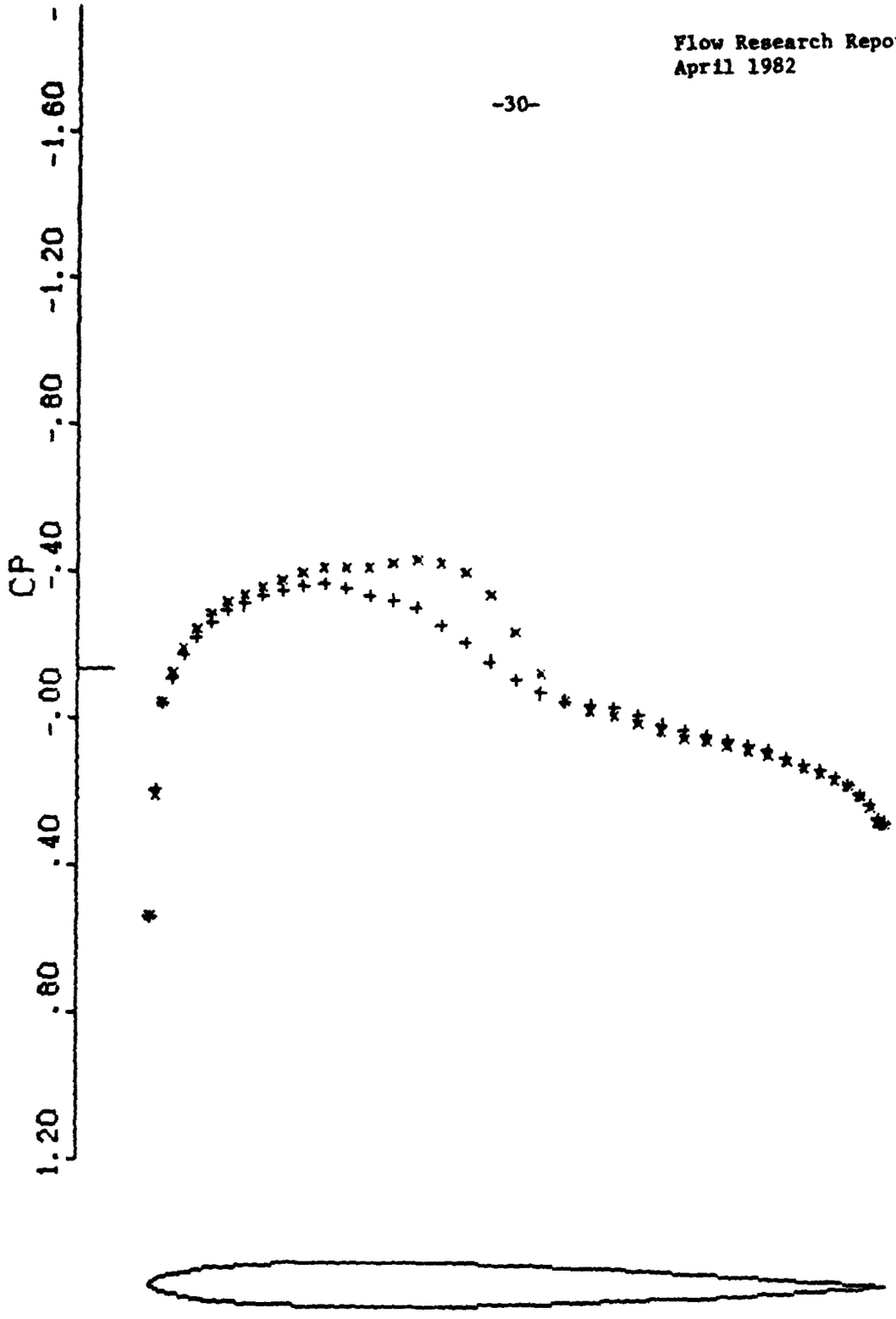

WINGBODY - TRANSONISK VINGE - SAAB-CYL (TWT)
MACH 0.925 ALPHA 1.000
Z 1.45 CL 0.0364 CD -0.0036

Figure 21. SAAB Tail Pressure

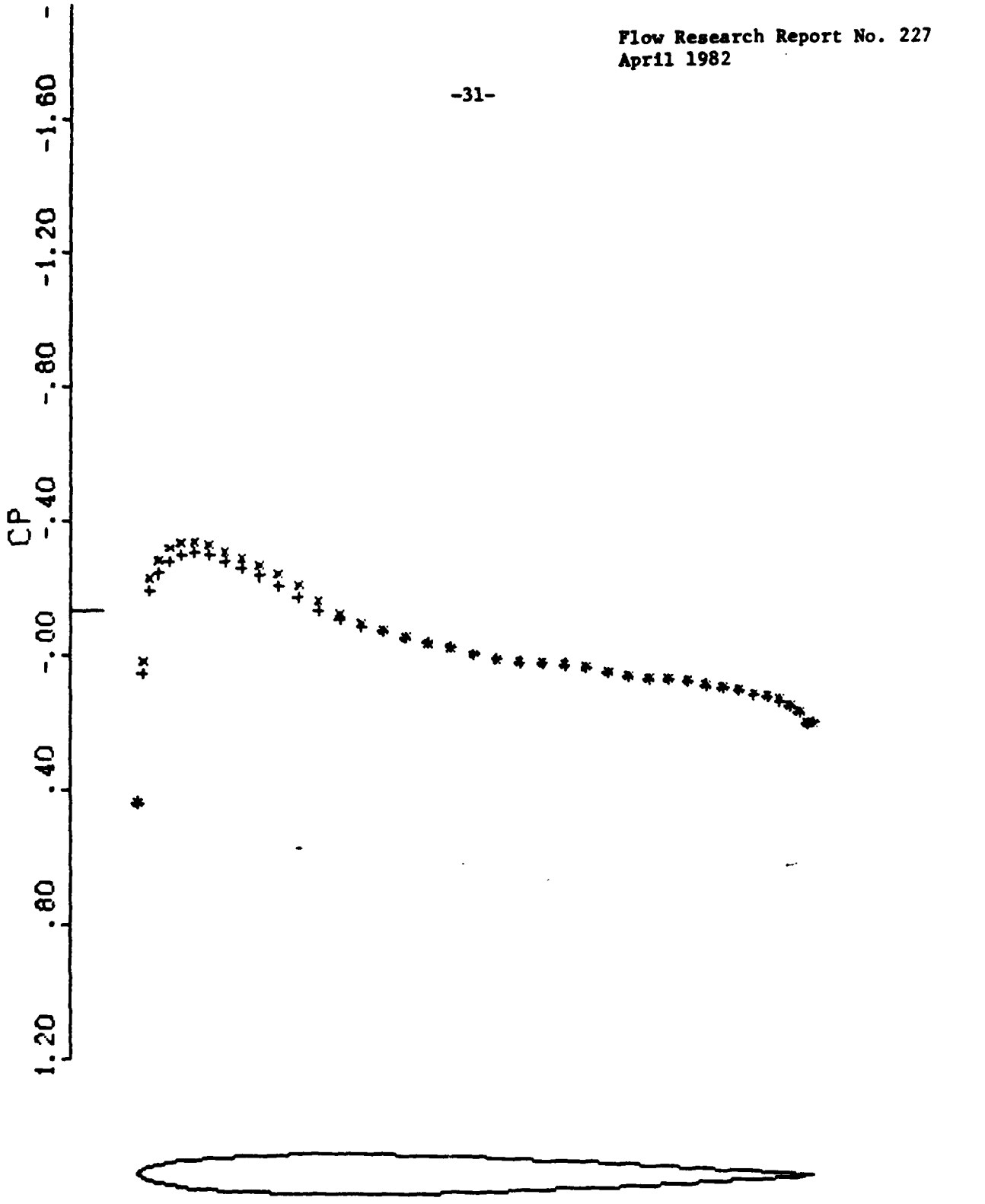

Figure 22. SAAB Tail Pressure

5. Conclusions

The present work demonstrates that the basic wing-body code can be extended to include other major components of a realistic aircraft by using an embedded mesh with interactive computations. The interaction between modules does not substantially affect the rate of convergence. Results for closely coupled wing-body-tail configurations show that the method is stable and produces the expected trends. Comparison with wind tunnel data for wing-tail configurations should be made when available to test the accuracy of the method. The program can provide designers with an accurate method for assessing tail designs under transonic flight speeds. For very closely coupled configurations, however, the method may fail because there may not be enough space between the wing and the tail for generating an embedded C-type mesh around the tail. Another mesh system, such as a unified grid with an H-type mesh, may be required (see Huynh and Jou, 1982). However, the concepts of overlapping meshes and interactive iterations demonstrated here can be of great value in any grid system where local accuracy is required.

References

Huynh, H., and Jou, W.-H. (1982) "Singularity Embedding Method in Potential Flow Calculations," to be published in the AIAA/ASME Third Joint Thermophysics, Fluids, Plasma and Heat Transfer Conference Proceedings, June.

Jameson, A., and Caughey, D. (1977) "A Finite Volume Method for Transonic Potential Flow Calculation," Proceedings of the AIAA Third Computational Fluid Dynamics Conference.

Mercer, J. E., Jou, W.-H., Caughey, D. A., Jameson, A., and Nixon, D. (1980) "Development of Finite Volume Methods for Three-Dimensional Transonic Flows," Flow Research Report No. 166.


DAT
ILM